Structure, Vol. 13, 953–962, July, 2005, ©2005 Elsevier Ltd All rights reserved. DOI 10.1016/j.str.2005.04.017

The Solution Structure of a Transient Photoreceptor Intermediate: Δ25 Photoactive Yellow Protein

Cédric Bernard,[1,3] Klaartje Houben,[1,4] Nocky M. Derix,[1] David Marks,[1] Michael A. van der Horst,[2] Klaas J. Hellingwerf,[2] Rolf Boelens,[1] Robert Kaptein,[1,*] and Nico A.J. van Nuland[1,5]

[1]Department of NMR Spectroscopy
Bijvoet Center for Biomolecular Research
Utrecht University
Padualaan 8
3584 CH Utrecht
The Netherlands

[2]Laboratory for Microbiology
Swammerdam Institute for Life Sciences
BioCentrum Amsterdam
University of Amsterdam
Nieuwe Achtergracht 166
1018 WV Amsterdam
The Netherlands

Summary

The N-terminally truncated variant of photoactive yellow protein (Δ25-PYP) undergoes a very similar photocycle as the corresponding wild-type protein (WT-PYP), although the lifetime of its light-illuminated (pB) state is much longer. This has allowed determination of the structure of both its dark- (pG) as well as its pB-state in solution by nuclear magnetic resonance (NMR) spectroscopy. The pG structure shows a well-defined fold, similar to WT-PYP and the X-ray structure of the pG state of Δ25-PYP. In the long-lived photocycle intermediate pB, the central β sheet is still intact, as well as a small part of one α helix. The remainder of pB is unfolded and highly flexible, as evidenced by results from proton-deuterium exchange and NMR relaxation studies. Thus, the partially unfolded nature of the presumed signaling state of PYP in solution, as suggested previously, has now been structurally demonstrated.

Introduction

The photoactive yellow protein (PYP) is a water-soluble photoreceptor of *Ectothiorhodospira* (or *Halorhodospira*) *halophila*, a motile, alkalophilic, and halophilic bacterium. *E. halophila* responds to blue light by avoiding exposure to harmful UV light (Meyer, 1985; Sprenger et al., 1993). This behavior is wavelength-dependent, with a maximum at 446 nm. The absorption maximum of PYP is also at 446 nm and, therefore, PYP is thought to play a key role in the negative phototaxis of *E. halophila*. PYP was proposed to be the structural prototype for the three-dimensional fold of the PAS domain (Pellequer et al., 1998), a structural entity that has been identified in proteins from all three kingdoms of life (i.e. in the *Bacteria*, the *Archaea*, and the *Eucarya*). Per-Arnt-Sim (PAS) is an acronym for the three proteins that were the first to be identified to contain a PAS domain: the *Drosophila* period clock protein (Per) (Crews et al., 1988), vertebrate aryl hydrocarbon receptor nuclear translocator (Arnt) (Hoffman et al., 1991), and *Drosophila* single minded protein (Sim) (Crews et al., 1988). Proteins containing PAS domains often possess a multidomain architecture and are involved in processes of signal transduction in the cell in response to changes in the environmental or intracellular conditions (Taylor and Zhulin, 1999). This makes these domains important signaling modules that monitor changes in light, redox potential, oxygen, small ligands, and overall energy level of a cell.

PYP has a chromophore, *p*-coumaric acid, covalently linked by a thiol-ester bond to the unique cysteine (Cys69) of the protein (Baca et al., 1994; Hoff et al., 1994a). Upon irradiation with blue light, PYP undergoes a photocycle (Figure 1A), whereby the chromophore changes its configuration about the double bond from *trans* to *cis* and becomes protonated upon formation of the long-lived, blue-shifted intermediate (pB, also known as I_2, PYP_M) (Hoff et al., 1994b; Meyer et al., 1987). As the pB intermediate is the most stable of the photocycle (its halftime lies in the subsecond time scale for wild-type PYP [WT-PYP]), it is believed that this is the signaling state of the protein. Within 1 s, PYP relaxes from the intermediate state (pB) back to the ground state (pG) (Hoff et al., 1994b; Meyer et al., 1987). The structure of PYP in the pG state has been elucidated through both crystallography (Borgstahl et al., 1995) and nuclear magnetic resonance (NMR) spectroscopy (Düx et al., 1998). PYP consists of four segments: (1) the N-terminal cap containing two α helices (α1 and α2); (2) a PAS core containing three β strands and two α helices (β1, β2, α3, β3, and α4); (3) a helical connector (α5); and (4) a β scaffold (β4, β5, and β6), as shown in Figure 1B. Earlier NMR studies on WT-PYP showed that, in solution, the protein exhibits dramatic chemical exchange behavior upon illumination, resulting in the loss of about 40% of the amide signals in the heteronuclear single-quantum coherence (HSQC) spectrum of the pB state. Analysis of ^{15}N chemical shift perturbations clearly showed that the entire molecule is affected upon illumination, with a region of major perturbation being the N-terminal part, helices α1, α2, and α3, and the first turn of helix α4, parts of strands β1 and β6 of the central antiparallel β sheet, and the chromophore-containing loop (Rubinstenn et al., 1998). These observations led to the conclusion that the protein partly unfolds upon formation of the light-induced pB state and hampered resolution of its spatial structure. This partial unfolding was not observed in the crystalline environ-

*Correspondence: kaptein@nmr.chem.uu.nl
[3]Present address: Architecture et Fonction des Macromolécules Biologiques, UMR6098, Centre National de la Recherche Scientifique, 31 chemin Joseph Aiguier, 13402 Marseille cedex 20, France.
[4]Present address: Institut de Biologie Structurale Jean-Pierre Ebel, Laboratoire de Résonance Magnétique Nucléaire, 41 rue Jules Horowitz, 38027 Grenoble Cedex 1, France.
[5]Present address: Departamento de Química Física, Facultad de Ciencias, Universidad de Granada, Campus Fuentenueva s/n, 18071 Granada, Spain.

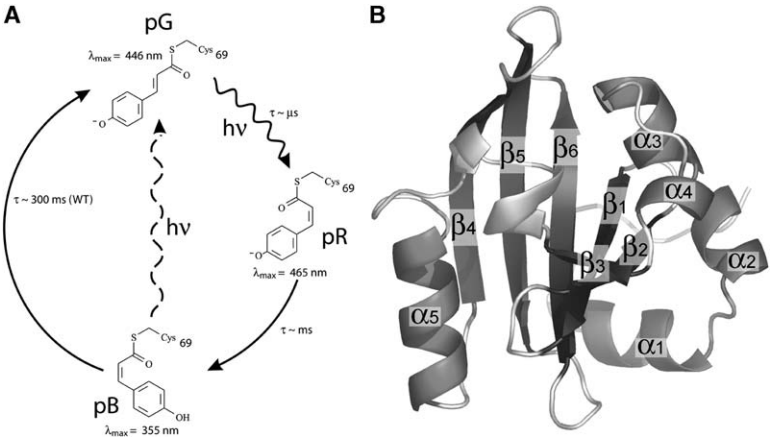

Figure 1. Photocycle and Structure of WT-PYP

(A) Simplified light cycle of WT-PYP. The different chromophore orientations, the time scale of each step, and the wavelengths of maximal absorbance are indicated.

(B) Representation of the crystal structure of WT-PYP (PDB 2PHY), in which β strands and α helices are shown and labeled as referred to in the text.

ment: only small structural differences between pG and pB were observed, and were found to be limited to the chromophore region (Genick et al., 1997). The same observation holds for the light-oxygen-voltage (LOV) class of PAS domains, where minimal changes were reported after crystallographic studies (Crosson et al., 2003; Fedorov et al., 2003) in contrast to spectroscopic studies (Corchnoy et al., 2003; Harper et al., 2003; Salomon et al., 2001; Swartz et al., 2002) that suggested more pronounced structural changes upon illumination of the LOV domain in solution.

Severe NMR line-broadening was the phenomenon that precluded a detailed structure analysis of pB of WT-PYP. Therefore, a truncated form of PYP, lacking the 25 N-terminal residues (Δ25-PYP), was analyzed (van der Horst et al., 2001). Δ25-PYP is a stable and photochemically active form of PYP that undergoes a very similar photocycle as the WT-PYP (van der Horst et al., 2001; Hendriks et al., 2002), although the rate of the recovery reaction in its photocycle is substantially lower. This slower recovery (halftime of 10 min for Δ25-PYP instead of 300 ms for WT-PYP) allows an almost quantitative accumulation of the pB state upon continuous and low-power illumination. In this article, we show that truncation of the protein has shifted the time scale of internal dynamics in the protein, resulting in sharpening of the broad NMR signals that hampered the study of the intermediate pB state of WT-PYP. The crystal structure of Δ25-PYP in the pG state has been reported (Vreede et al., 2003) and showed that the removal of the first 25 residues does not significantly affect the overall fold of the PAS domain core. It was thus suggested that Δ25-PYP represents the minimal PAS domain core.

Here we present the NMR solution structure of both the dark pG state and the light-induced pB state of Δ25-PYP and compare these states in terms of structure and dynamics. The results show that the central β sheet does not change its structure upon illumination, in contrast to the region flanking the β sheet that is partially unfolded. This is supported by proton-deuterium H-D exchange experiments that show a loss of hydrogen bonds in this region, and ^{15}N relaxation measurements that reveal increased flexibility. The partial unfolding of the PYP structure is believed to be an essential event in the signal-transduction process.

Results

Resonance Assignment and Chemical Shift Perturbation

All backbone amide proton ^{15}N spin pairs of pG could be assigned, whereas 94% could be assigned for pB; ^{1}H-^{15}N assignment for residues F28, C69, S72, T95, Y98, and M100 were still missing due to overlap or exchange broadening. With the exception of the labile side-chain protons of lysine and arginine residues, 95% and 85% of all observable protons were assigned in pG and pB, respectively.

The ^{15}N-HSQC spectra of pG and pB show good dispersion of the ^{1}H-^{15}N cross-peaks (Figure 2). However, in pB the dispersion of the cross-peaks is less wide and the line width of the peaks is broader than in pG, indicating a less well-defined structure of pB compared to pG. The number of cross-peaks in the spectrum of pB is closely similar to that in the pG spectrum, indicating that Δ25-PYP does not show the strong exchange phenomena that were observed in the pB spectra of WT-PYP (Rubinstenn et al., 1998). The weighted chemical shift differences in the ^{1}H-^{15}N chemical shifts between pG and pB for Δ25-PYP and WT-PYP have been analyzed: for Δ25-PYP, the three regions encompassing residues 42-58, 63-79 and 97-103 are strongly affected by the illumination (see Figure S1 in the Supplemental Data available with this article online). These three regions correspond to the residues that are most subject to exchange broadening in WT-PYP pB, where they were thus left unassigned (Craven et al., 2000). The analysis of the composite chemical shift differences, therefore, indicates that Δ25-PYP and WT-PYP react in a similar way to light, except for the N terminus, which is lacking in Δ25-PYP.

H-D Exchange

The protection factors obtained from H-D exchange experiments are shown in Figure 3 for both pG and pB of Δ25-PYP, and for pG of WT-PYP. The long recovery time of the reaction from pB back to pG enabled direct de-

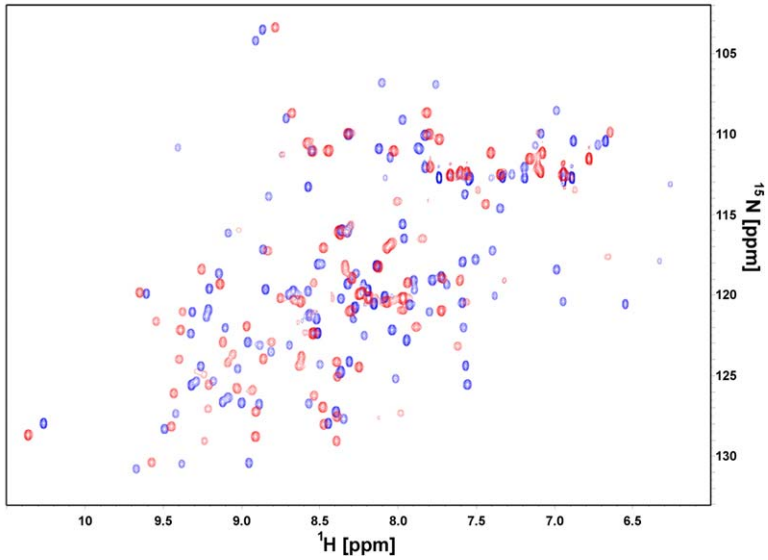

Figure 2. Overlay of ^{15}N-HSQC Spectra of the Δ25-PYP pG State and pB State

Overlay of ^{15}N-HSQC spectra of the Δ25-PYP pG state (in blue) and pB state (in red) recorded at 293 K on a Bruker Avance 750 MHz spectrometer.

tection of stable hydrogen bonds within the signaling (i.e., pB) state of Δ25-PYP; upon illumination, 20 amides showed H-D exchange slow enough to be analyzed compared to 52 for the pG state. This indicates that, upon illumination, the hydrogen-bonding network of the protein is largely perturbed. Only the amide protons in the first and last two β strands retain protection against exchange. A different method was previously used to follow the H-D exchange process in pB of WT-PYP, as continuous illumination was not possible due to the fast recovery in WT-PYP. In those experiments, about 14 amide protons were found to exhibit a significantly faster exchange rate upon illumination for WT-PYP (Craven et al., 2000; Rubinstenn et al., 1999). These residues are marked with an asterisk in Figure 3. All these residues exchange within the dead time of the experiment in the pB state of Δ25-PYP, except for M109, which still shows high protection in the pB state. This might be explained by local rearrangements around this residue, as it is positioned in the region that is flanked by the N-terminal part in WT-PYP, which is no longer present in Δ25-PYP. In contrast to what was observed in WT-PYP, the α helix 44–49 (α3 in WT-PYP) in the pG state of Δ25-PYP does not show any protection against H-D exchange, which is also most likely due to the absence of the N-terminal part, as these regions are in close contact in the WT-PYP structure.

Solution Structure of the pG and pB States of Δ25-PYP

The structural statistics for the final pG and pB structure are presented in Table 1. The structure of these states of Δ25-PYP were determined on the basis of 1464 (pG) and 1029 (pB) unambiguous restraints divided into 548 and 520 intraresidual, 418 and 287 sequential, 179 and 61 medium-range, and 319 and 161 long-range restraints for pG and pB, respectively (see Figure S2 online). For the pG state, the distribution of restraints is in agreement with the occurrence of residues in a secondary structure element (i.e., a higher number of restraints for residues in β strands or α helices and fewer restraints for those in loop regions). Despite the fact that region 44–49 in pG clearly showed nuclear Overhauser enhancement (NOE) patterns typi-

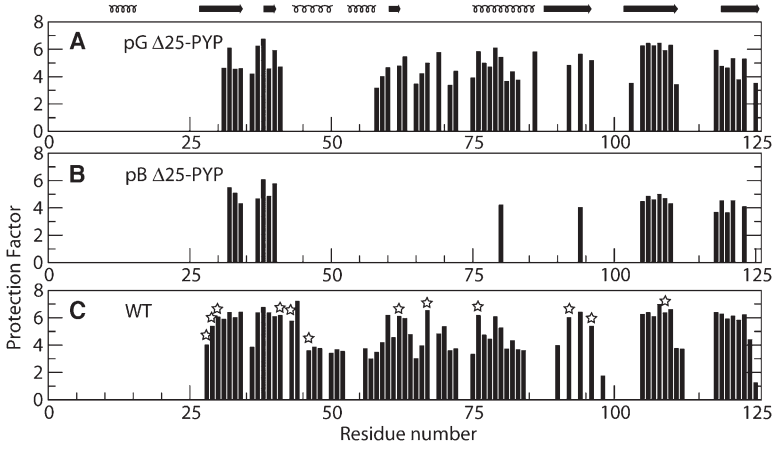

Figure 3. H-D Exchange Experiments

Logarithmic plot of the protection factor per residue for (A) Δ25-PYP pG, (B) Δ25-PYP pB, and (C) WT. The residues that showed a distinct difference in exchange rate upon illumination in WT-PYP (Craven et al., 2000) are marked with an asterisk. The secondary structure of PYP, as determined in solution (Düx et al., 1998), is shown above the figure.

Table 1. Structural Statistics for Δ25-PYP in the pG and pB States

	pG	pB
Rmsd (Å)		
Backbone heavy atoms, secondary structure elements[a]	0.85 ± 0.23	0.75 ± 0.21
All heavy atoms, secondary structure elements[a]	1.37 ± 0.34	1.37 ± 0.26
Backbone heavy atoms, all residues	1.18 ± 0.30	3.77 ± 1.06
All heavy atoms, all residues	1.74 ± 0.43	4.74 ± 1.22
Energies (kcal mol^{-1})		
VdW	–237 ± 65	–109 ± 71
Elec	–3905 ± 93	–3678 ± 113
Rmsd from idealized covalent geometry		
Bonds (Å)	$4.53 \times 10^{-3} \pm 1.35 \times 10^{-4}$	$5.23 \times 10^{-3} \pm 1 \times 10^{-4}$
Angles (°)	0.69 ± 0.02	0.75 ± 0.01
Improper (°)	1.68 ± 0.14	1.68 ± 0.09
Dihe (°)	41.4 ± 0.3	42.0 ± 0.4
Rmsd from experimental restraints		
NOE (Å)	$2.38 \times 10^{-2} \pm 1.5 \times 10^{-3}$	$3.72 \times 10^{-2} \pm 1.6 \times 10^{-3}$
cdih (°)	0.32 ± 0.14	0.96 ± 0.11
Unambiguous restraints	1464	1029
Intraresidual	548	520
Sequential	418	287
Medium range ($2 < \|i - j\| \leq 4$)	179	61
Long range ($\|i - j\| \geq 5$)	319	161
Other restraints		
Ambiguous restraints	87	214
H bonds	30	20
TALOS predicted dihedrals	61	46
Chromophore-protein NOEs	16	0
Restraints violations in more than 50% of the structures[b]		
NOE > 0.5 Å	0	0
cdih > 5°	0	2
Ramachandran plot (%)		
Favored regions	76.5	69.5
Additionally allowed regions	20.2	26.1
Generously allowed regions	2.3	2.7
Disallowed regions	1.0	1.7

[a] Regular secondary structure elements include residues 29–34, 39–41, 44–49, 76–85, 89–96, 103–112, and 117–124 in the pG state, or residues 30–34, 39–41, 79–85, 90–95, 104–111, and 117–124 in the pB state.
[b] No dihedral angles restraint was violated by more than 5.9°.

cal for α-helical structure, the total number, and therefore the structural definition, of this region is substantially lower than that of other helices, in agreement with the fast H-D exchange in this region. The number of restraints per residue is generally lower for pB over the whole sequence, and does not seem to be restricted to specific regions of the protein. However, some parts of pB, such as regions 63–78 and 95–100, show an almost complete loss of NOEs. In order to characterize specific contacts between the chromophore and the rest of the protein, we conducted isotope-filtrated experiments. We obtained 17 chromophore-protein NOE's for pG, and all were confirmed by occurrence of such contacts in the crystal structure of Δ25-PYP (Vreede et al., 2003).

Figure 4 presents the family of 20 structures of Δ25-PYP in the pG (Figure 4A) and pB state (Figure 4B) that satisfy the experimental restraints. The structure of pG is composed of a regular five-stranded β sheet, encompassing residues 29–34 (β1), 39–41 (β2), 89–96 (β3), 103–112 (β4), and 117–124 (β5), and two α helices (residues 44–49 for α3 and 76–85 for α5, helices being numbered as in WT-PYP). Other secondary structure elements, such as a β strand from residues 59–61 and three helices encompassing residues 54–57, 62–65, and 68–70, were detected in a few structures. The structure of pG is well-defined, as is reflected by the low rmsd values, and is of good quality, as indicated by the energetic terms and Ramachandran statistics (Table 1). The region 42–56, that comprises α helix 44–49, shows higher rmsd values and is less well-defined (Figure 4A), reflecting higher disorder and flexibility. If this helix is omitted, the rmsd on secondary structure elements is reduced to 0.67 ± 0.18 and 1.28 ± 0.32 Å for backbone atoms and all heavy atoms, respectively. More evidence for the increased flexibility of the protein in solution in this region comes from the lack of protection of the amide protons (H-D exchange) and the observed flexibility from NMR relaxation experiments that are discussed below.

The superposition of the best 20 structures of the pB state of Δ25-PYP is displayed in Figure 4B. It is readily apparent that pB is much less well-defined than pG: Three regions that encompass residues 42–58, 63–78, and 96–103 adopt several orientations that are all consistent with the experimental restraints. As the presence of conformational averaging in flexible loops can complicate the calculation of a single set of structures, we also checked for the presence of conformational averaging by performing ensemble-average refinement with complete cross-validation against the number of conformers (Bonvin and Brunger, 1996). This procedure indicated that a single conformer was sufficient to sat-

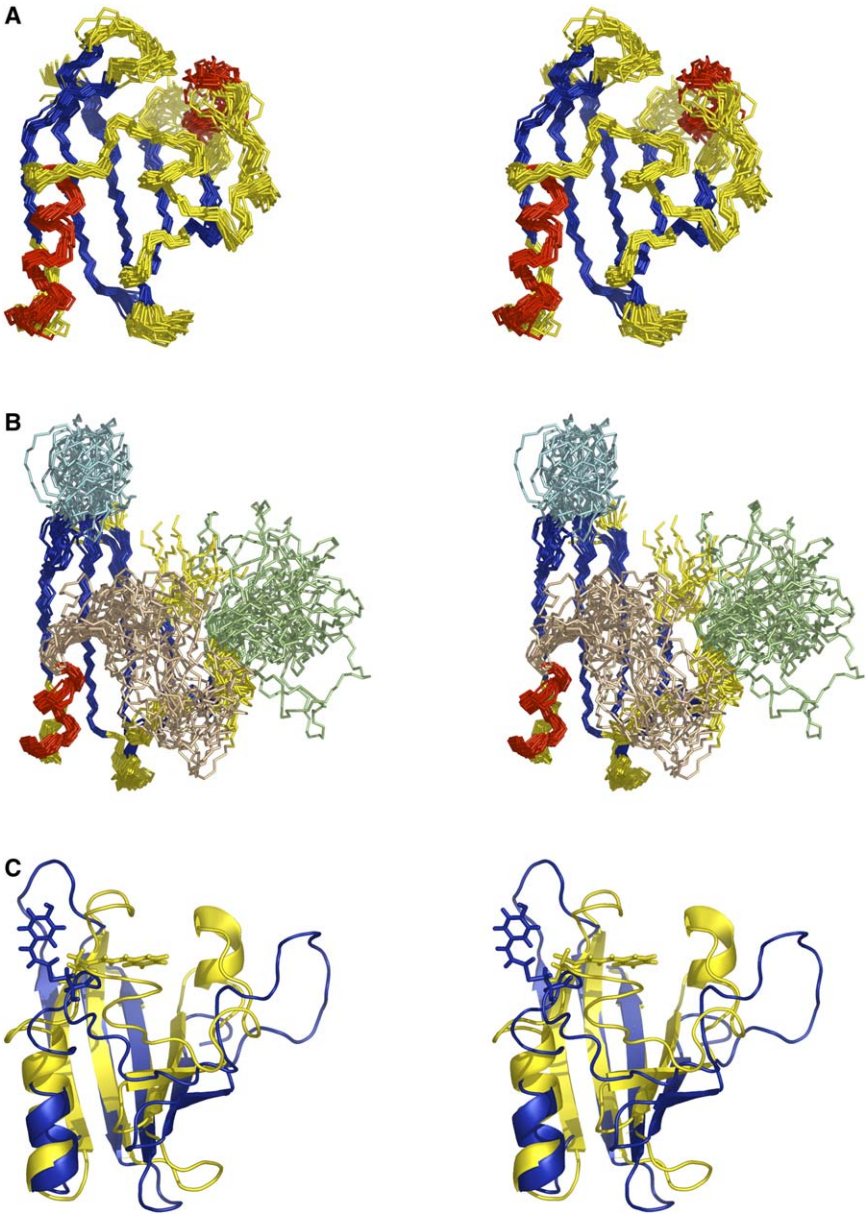

Figure 4. Stereoview of the Ensemble of Solution Structures of the pG and pB States of Δ25-PYP

Superposition of the twenty best structures of Δ25-PYP in the pG (A) and the pB states (B). Structures were superimposed on the backbone atoms of the secondary structure elements, including residues 29–34, 39–41, 76–85, 89–96, 103–112, and 117–124 in the pG state, or residues 30–34, 39–41, 79–85, 90–95, 104–111, and 117–124 in the pB state. Secondary structure elements, as detected by PROCHECK, are represented and colored in blue for the β strands and red for α helices. The three flexible regions encompassing residues 43–58, 62–78, and 96–103 of pB are colored in green, wheat, and orange, respectively. For both states, the chromophore is represented in sticks. (C) Superposition of the closest to the mean structures of pG and pB. The structures were superimposed on the backbone atoms of the residues involved in the β sheet in the pB state (30–34, 39–41, 90–95, 104–112, and 117–124). pG and pB are colored in yellow and blue, respectively. The chromophore is represented by sticks.

isfy the experimental restraints (data not shown). The structure of pB can be described as being composed of a regular five-stranded β sheet, encompassing residues 30–34 (β1), 39–41 (β2), 90–95 (β3), 104–111 (β4), and 117–124 (β5), and one α helix from residues 79–85 (corresponding to α5 in WT-PYP). Concerning the secondary structure elements, the β sheet defined in pG is conserved in pB, even if some of the constituent strands are shorter by one or two residues. All α helices of the protein are destabilized in pB: α helix 44–49, already identified as less stable in pG, is absent, as confirmed by the lack of typical α-helical NOEs for these residues. Interestingly, the α helix that comprises residues 76–85 in pG is shorter in pB; residues 79–85 constitute a well-defined α helix, whereas residues 76–78 are flexible with few sequential medium- and long-range restraints. No other regular element of secondary structure can be detected, except one α helix (residues

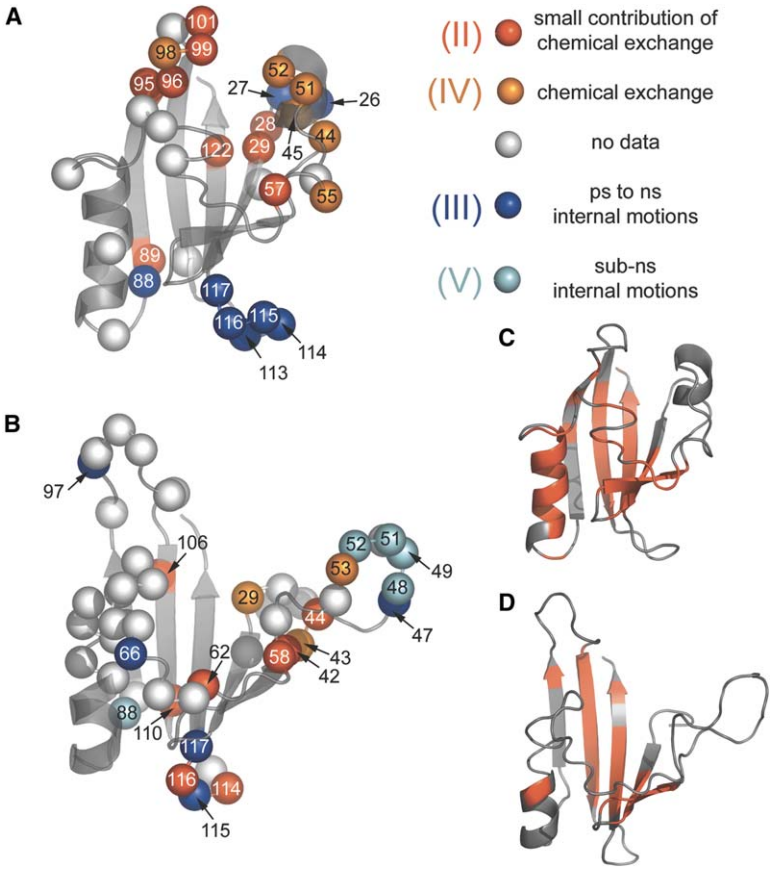

Figure 5. Backbone Dynamics and Protected HN Groups Mapped on the Structure of pG and pB of Δ25-PYP

Data points were divided over four (pG) or five groups (pB) depending on their motional behavior. The different groups are mapped on the structure of (A) pG and (B) pB. The residues of group I are colored in gray; all residues of other groups are represented with a sphere colored in red for group II, in blue for group III, in orange for group IV, and, in the case of pB, in cyan for group V. The group numbers in brackets, together with the observed type of internal motions, are indicated. The protection factors extracted from H-D exchange are highlighted in the structure of (C) pG and (D) pB. The amide protons for which a protection factor was determined are colored in red.

54–56) in one of the 20 best structures. Due to the presence of disordered regions, the Ramachandran plot is of lower quality than that of the pG state. The calculated structures show no NOE violations greater than 0.5 Å, but do show two dihedral angle restraint violations greater than 5° (with a maximum of 5.9°). The plot of rmsd versus the sequence indeed shows low values for secondary structure elements and high values (up to 7 Å) for the less well-defined parts of the protein (see Figure S2D online). No NOEs between the chromophore and the protein, which were observed for pG, could be collected for pB. In pG, the chromophore is well-defined and buried in the so-called chromophore binding pocket, while in pB, it is solvent-exposed and linked to a very flexible loop. Figure 4C displays the superposition of the structure closest to mean on Δ25-PYP in both states and clearly emphasizes the differences that have been described above.

Relaxation Rate Measurements

The NMR relaxation rates of ^{15}N nuclei in the protein backbone are sensitive probes of the overall rotational diffusion of a protein, as well as of the local dynamics of the protein backbone. From the average ^{15}N relaxation parameters for 72 rigid residues of pG (see Figure S3 online), the apparent correlation time was estimated to be 7.7 ± 0.5 ns. Based on their relaxation rates in the pG state, we could identify four different groups of residues that display a similar dynamic behavior (see Figure S4 online), and are mapped by colored spheres on the structure of Δ25-PYP in Figure 5A. Group I contains residues in the core of the protein, including the β sheet, the helix α3, and the chromophore binding loop (gray ribbon in Figure 5). The residues of group II have slightly higher transversal R_2 relaxation rates, which could be due to either anisotropic tumbling or a small contribution of conformational exchange. However, the rotational diffusion anisotropy in the pG state is calculated to be rather small (1.2–1.3) and, as most residues in group II are located in loops and do not all have the same NH orientation, it is more likely that the higher R_2 rates for these residues are caused by a small contribution of conformational exchange. Group III contains residues that are flexible on a fast (ps-ns) time scale, as evidenced by low heteronuclear NOE values as well as low R_1 and R_2 relaxation rates. The residues in the last group (IV) all have R_2 relaxation rates higher than 12 s^{-1}, which is indicative of a strong contribution of conformational exchange.

Although the protein structure in the pB state is partially unfolded, the ^{15}N relaxation rates of amides located in the folded parts of the protein do give information on the rotational diffusion of the protein. The average relaxation parameters for pB, calculated on the basis of 29 residues located in rigid parts of the structure, result in an apparent correlation time of 8.7 ± 0.7 ns. This higher correlation time for pB compared to pG (increase of about 13%) results from a global increase of the average R_2 and decrease of the average R_1 values in pB, and might be due to an increase of structural volume; hydrodynamic calculations using HYDRONMR (Garcia de la Torre et al., 2000) of both the pG and pB

ensembles of structures reveal an increase in average volume of 11% between pG (20,995 ± 757 Å^3) and pB (23,377 ± 1,271 Å^3). The increase in the spread of R_2 and R_1 relaxation rates indicates a small increase in rotational diffusion anisotropy in the pB state.

As for pG, based on the ^{15}N relaxation rates in the pB state (see Figure S3 online) we identified different groups of residues that display distinct motional behavior, which are color-coded on the structure of pB (Figure 5B). However, in the case of pB, one extra group (group V) that displays sub-ns motion could be identified, as evidenced by low heteronuclear NOE values and R_2 relaxation rates, but increased R_1 relaxation rates. For the stretch of residues ranging from 67 to 79, no accurate relaxation rates could be determined due to overlap.

Discussion

Structure and Dynamics of the pG State of Δ25-PYP and Comparison with WT-PYP

Here we present the high-resolution structure of the pG state of Δ25-PYP determined by NMR. The structure is very similar to the NMR structure of the WT protein (secondary structure rmsd of 1.42 Å), as well as to the X-ray structure of Δ25-PYP (secondary structure rmsd of 1.36 Å). The lack of the N-terminal part seems to have little effect on the rest of the structure, except for the helices comprising residues 44–49 (α3) and residues 54–57 (α4 in WT-PYP) that are less stable in Δ25-PYP, as these regions show conformational exchange in relaxation measurements (Figure 5A) and less protection in H-D exchange experiments (Figure 5C). In the helix 44–49, a strong contribution of conformational exchange is found for the flanking residues Ala44, Ala45, Thr50, and Gly51, confirming that this helix is not well-defined in solution. In WT-PYP, this helix is well-defined and shows no conformational exchange. The exchange observed in Δ25-PYP is thus presumably caused by the removal of the N-terminal 25 residues, which leads to the loss of two hydrogen bonds with the backbone amides of Asn43 and Ala44. Moreover, a few hydrophobic contacts with the rest of the protein are lost: in WT-PYP, residues Phe6, Ile11, Leu15, and Leu23 are close to residues Leu26, Phe28, Trp119, and Phe121. In helix 54–57, which was identified in the X-ray structure of both WT-PYP and Δ25-PYP, but which was defined in only 30% of the WT-PYP NMR ensemble of structures, is present only in 10% of the Δ25-PYP NMR structures. In this helix in pG of Δ25-PYP, Lys55 exhibits ms-μs conformational exchange and—although less pronounced—Val57 as well, whereas in WT-PYP, Lys55 exhibits ns-ps motion, indicating a shift in the time scale of dynamics between WT-PYP and Δ25-PYP. As in WT-PYP, Leu88 in the stretch between α5 and β3 shows high-amplitude fast motion and, moreover, the adjacent residue (Asn89) in Δ25-PYP displays slow conformational exchange. In the loop connecting β3 and β4 (97–102), many residues have high R_2 values, indicative of conformational exchange, which is most prominent for Tyr98. In pG of WT-PYP, conformational exchange is observed for Gln99. In both WT-PYP and Δ25-PYP, the loop (113–116) between β4 and β5 is flexible on a fast time scale. In the β sheet, both Gly29 (from β1) and Val122 (from β5)—that are facing each other—show a small contribution of conformational exchange (group II). This indicates a slightly lower stability of these positions in the β sheet.

In summation, the dark-state structures of WT-PYP and Δ25-PYP are practically the same; only subtle differences are observed in the dynamics of the protein and in the stability of helix 44–49.

Structure and Dynamics of Δ25-PYP pB and Comparison with Δ25-PYP pG

The more favorable spectroscopic properties and photocycle kinetics, due to a change in the time scale of local dynamics brought about by removing the 25 N-terminal residues, allowed us to solve the solution structure of the pB state of Δ25-PYP. Recently, NMR studies in solution of a LOV2 domain indicated that upon illumination of this protein there occurs mainly unfolding of the C-terminal helix (Harper et al., 2003). These studies also showed that the PAS core (AsLOV2Δ [AsLOV2 lacking the C-terminal helix]) responds in the same way to light as the full-length AsLOV2 protein (Harper et al., 2003). Similarly, Δ25-PYP also corresponds to a single PAS domain. The structure of the pB state of Δ25-PYP is the first solution structure of a photocycle transient intermediate and can be described as a partially unfolded protein. This latter fact is derived from the dramatic loss of protection against H-D exchange, from a substantial decrease in the number of NMR restraints, and from an increase in local backbone flexibility. When comparing the structures of Δ25-PYP in the pG and pB state, the main event occurring upon illumination is an unfolding of all α helices of the protein, except half of α5, whereas the β sheet is practically unaltered. Clearly, helix α3 (44–49) that is already not well-defined in pG, is absent in pB, consistent with fast H-D exchange in this region (Figure 5D) and the observed ms motion for residues 42–44, sub-ns flexibility for residues 48–52, and fast ps-ns time scale motion for Gly47 (Figure 5B). As discussed above, in pG the residues at the edges of this helix display slow conformational exchange, presumably due to the removal of the N-terminal tail, which induces a destabilization of this helix. Hence, the destabilization of this helix may cause the helix to unfold more readily upon illumination, and may therefore be one of the factors responsible for the slower pG-state recovery of Δ25-PYP. It should be noted that Glu46, which makes a hydrogen bond with the chromophore in pG that is broken in pB, is located in helix α3. In the same region, Asp53 and Ile58 in pB display slow conformational exchange, which is mainly observed for Lys55 in pG. Studies on WT-PYP have shown that in the pB state and in the low-pH state of PYP (pB-dark), a dramatic loss of signal intensity is observed for the region encompassing residues 43–58. In WT-PYP, this signal loss is presumably caused by conformational exchange on a time scale incompatible with the NMR time scale, and clearly the time scale of this motion in Δ25-PYP has shifted to an NMR-observable time scale.

In pG residues 76–85 form part of helix α5, while in pB this helix only encompasses residues 79–85. The preceding loop 62–79 is ill-defined in the pB solution structure; however, due to line-broadening and resonance overlap, no reliable information on the motional

behavior of this loop is available. Nevertheless, Phe62 and Val66 exhibit distinct slow conformational and ps-ns motions, respectively. The flexibility of the loop that covalently binds the chromophore precludes the latter having a well-defined orientation. This fact is in strong contrast with the crystal structure of WT-PYP pB, where low B factor values are found for this loop. As in pG, Leu88 is also flexible in pB, although the time scale of motion is slightly slower. Due to lack of data, a rigorous analysis of the loop 97–102 is impossible, but Asp97 displays ps-ns motion. The position of this loop, and, in particular, of M100, is crucial for catalysis of regeneration of the pG state from pB (Devanathan et al., 1998). In the loop (113–116) between β4 and β5, all residues show flexibility on a fast time scale as was observed in pG, only for Ser114 and Asp116 there is also evidence of a contribution of conformational exchange in pB.

There is a considerable discrepancy in the literature concerning the actual volume increase of PYP when entering the pB state. Whereas X-ray and neutron scattering (Imamoto et al., 2002) show a small net volume increase, photoaccoustic measurements (Takeshita et al., 2002) show a considerable increase of up to 60%. In this study, we show that the global overall correlation time of PYP, as obtained from NMR relaxation, is 13% higher for Δ25-PYP pB than for Δ25-PYP pG. This agrees with the computed increase of structural volume (11%) from hydrodynamic calculations of the structural ensembles.

Effect of the N Terminus on the Lifetime of the pB State

The absence of the N-terminal region dramatically increases the lifetime of the pB state. We suggest that the observed destabilization of the helix in Δ25-PYP comprising the residues Asn43 to Thr50 is related to this phenomenon. The protection factors, obtained from H-D exchange experiments of the pG state of Δ25-PYP, are substantially smaller for this helix than observed in WT-PYP. This helix is in close proximity to the N-terminal part in the WT-PYP structure, stabilized by a network of hydrogen bonds around Glu46 and Phe29. It has been shown previously that, upon illumination, this hydrogen bonding network is altered and that the N-terminal part subsequently unfolds into a "molten globule"-like state (Craven et al., 2000) characterized by exchange broadening of the spectra of WT pB. It was then proposed that the recovery process will proceed through a transition state, in which this essential part of the molecule is structured as in pG and presumably similar to the pB state trapped by X-ray crystallography. As the hydrogen bonding network between the helix comprising residues Asn43 to Thr50 and the N-terminal part is disturbed in Δ25-PYP, it is likely that this destabilizes the transition state with a concomitant increase in the height of the energy barrier for the pB-to-pG transition.

In conclusion, in the pB state of Δ25-PYP, the β sheet stays intact, whereas only half of helix 5 remains out of all the α helices, indicating a partial unfolding of the protein. In addition, the chromophore binding loop, which has a well-defined conformation in pG, is disordered in pB. Finally, the three main regions in WT-PYP pB that showed strong chemical exchange behavior correspond to the three flexible regions of Δ25-PYP pB. It is interesting to note that a recent modeling study of WT-PYP using "parallel tempering" (Vreede et al., 2005) shows also a partial unfolding of the pB state, resembling our observations on Δ25-PYP. The observed unfolding of Δ25-PYP upon illumination parallels the results of the NMR studies of the AsLOV2 domain (Harper et al., 2003). The general destabilization upon illumination of these two photosensors, which have very different chromophores, supports the view that partial unfolding and concomitant surface or peptide chain exposure is a prerequisite for the signaling state for PAS domains, as suggested by Harper et al. (2003). Nevertheless, the unfolding of the two sensors is quite distinct, with a locally affected helix C-terminal to the PAS core in the case of LOV2 and with more extensive unfolding events in the PAS core for Δ25-PYP. Whether this reflects the different signaling pathways in which these two sensors are involved is a question that can only be addressed upon availability of PAS domain-containing receptor complexes with their downstream partners.

Experimental Procedures

Sample Preparation

Uniformly ^{15}N-labeled and ^{15}N-^{13}C-labeled Δ25-PYP were expressed and purified as described previously (Vreede et al., 2003). All samples contained 50 mM phosphate buffer at pH 7.0, 90%/10% v/v H_2O/D_2O, and a protease inhibitor cocktail (complete, Roche Applied Science). Samples had a concentration of 1 mM.

NMR Experiments

All spectra were recorded on a Bruker Avance 500, 750, or 900 MHz spectrometer. All spectra were acquired at 293 K for both states of Δ25-PYP (i.e., with or without light). An Argon laser (Stabilite 2017, Spectra-Physics) with mechanical shutter connected to a glass fiber light guide was used to illuminate the sample in the probe of the spectrometer (Rubinstenn et al., 1999). The measured output used for total conversion from pG to pB was 20 mW, and continuous illumination was applied during all the experiments on the pB state. The sequential assignment in both the pG and the pB states was obtained according to standard methods (Sattler et al., 1999). The assignment of aromatic side-chain protons was achieved using nuclear Overhauser enhancement spectroscopy (NOESY) recorded in 100% D_2O. All spectra were processed with NMRPipe (Delaglio et al., 1995) and analyzed using NMRView (Johnson and Blevins, 1994). Chemical shifts have been deposited in the BMRB data bank with accession numbers 6321 and 6322 for pG and pB, respectively. As the chromophore itself was not ^{13}C-labeled, chromophore-protein NOEs were obtained by recording a ^{13}C-filtered NOESY as previously described (Zwahlen et al., 1997). Combined amide proton and nitrogen chemical shift differences were calculated using the following equation:

$$\Delta\delta_{ppm} = \sqrt{(\Delta\delta_{HN})^2 + \left(\frac{\Delta\delta_N}{6.51}\right)^2}.$$

H-D exchange experiments were performed by lyophilizing a ^{15}N-labeled sample and redissolving it in D_2O, thereby monitoring the loss of intensity of labile protons by recording sequential series of ^{15}N-HSQC spectra for a total recording time of 95 hr. The time between dissolving the lyophilized protein and the start of the first ^{15}N-HSQC experiment was 10 min for the experiment without illumination (pG) and 30 min for that with illumination (pB). Measured intensities were fitted to a single exponential decay, and the obtained rates were converted into protection factors using the method described previously (Bai et al., 1993, 1995).

^{15}N Relaxation Measurements

^{15}N T_1 and heteronuclear ^{1}H-NOE values were determined using the experiments described previously (Farrow et al., 1994). T_1 times were extracted from eight spectra with different values for the relaxation delay. The heteronuclear NOE was recorded in an interleaved fashion. The ^{15}N T_2 relaxation times were extracted from both CPMG (Meiboom and Gill, 1958) (recorded only for the pG state) and $T_{1\rho}$ (Peng et al., 1991) experiments. CPMG experiments were recorded using 10 different values for the relaxation delay with a field strength of 7.8 kHz (ν_{CPMG} = 1 kHz). The $T_{1\rho}$ experiments were recorded with varying lengths of an adiabatic spin-lock pulse (2.5 kHz). The number of ^{1}H 180° pulses during the relaxation period was adjusted to the relaxation delay used (Korzhnev et al., 2002). Relaxation parameters were extracted and analyzed with the program Curvefit (http://cpmcnet.columbia.edu/dept/gsas/biochem/labs/palmer/software/curvefit.html), using either a two- or three-parameter fitting, and a Monte Carlo simulation, to estimate the error. In the case of pB, the T_2 relaxation times were extracted from the $T_{1\rho}$ times according to:

$$\frac{1}{T_{1\rho}} = \frac{1}{T_1}\cos^2\theta + \frac{1}{T_2}\sin^2\theta,$$

where the angle, θ, is the angle between the effective field and the static magnetic field.

Structure Calculation

The automated assignment and structure calculations of both states of Δ25-PYP were performed with ARIA1.2 (Linge et al., 2001) using CNS (Brunger et al., 1998). The topallhdg5.3.pro (Linge et al., 2003) topology and parameter set was used based on the parallhdg parameters. The structural information used in each calculation was based on manual assignment of cross-peaks in the NOESY spectra in H_2O (also in 100% D_2O for pB) and 3D ^{15}N-NOESY-HSQC spectra, especially those of sequential residues and of all secondary structure elements of the protein. Additionally, TALOS (Cornilescu et al., 1999) dihedral restraints derived from $^{13}C\alpha$ chemical shifts and hydrogen bonds derived from the H-D exchange analysis were added as structural input during the calculations. At the end of each of the nine ARIA iterations, the structures were selected based on their NOE energy term. The NOEs, with the exception of those that had been manually assigned, were reassigned and recalibrated based on the 30 lowest energy structures and were rejected if violated in more than 50% and 30% of the structures for the first 5 and the last 4 iterations, respectively. A high-temperature torsion angle dynamics (TAD) stage consisting of 10,000 steps at 10,000 K was followed by an 8,000-step TAD cooling stage to a temperature of 2,000 K, a 10,000-step first Cartesian cooling stage to 1,000 K, and finally a 10,000-step second Cartesian cooling stage to 50 K. The number of calculated structures in the iterations was 150 for the first 8 iterations and 200 for the final iteration, with 30 and 50 structures, respectively, that were kept for the subsequent iteration. The structures were subjected to a final refinement protocol with explicit waters using the OPLS parameters (Jorgensen and Tiradorives, 1988), and the 50 lowest energy structures were analyzed in terms of violations, with respect to geometry using the program PROCHECK (Laskowski et al., 1996), and energy, resulting in a final set of 20 structures. The crystal structure of Δ25-PYP (Vreede et al., 2003) was used as a starting structure for the structure calculation of the pG state. For the pB state, the structure calculation was performed using two runs: In the first run, a linear structure was used as a starting structure, and in the second run, the lowest energy structure of the first run was used, using the final set of restraints of run 1. All structure representations were made with the program PYMOL (http://www.pymol.org/). The structural coordinates have been deposited in the Protein Data Bank with the following accession codes: 1XFN for pG and 1XFQ for pB.

Hydrodynamic Calculations

The volumes of the pG and pB state of Δ25-PYP were calculated with the program HYDRONMR (Garcia de la Torre et al., 2000) using a temperature of 293 K, a viscosity of 1.1 cP, and a radius of 3.2 Å for the spherical elements used to build the initial shell.

Supplemental Data

Supplemental data, including figures, are available at http://www.structure.org/cgi/content/full/13/7/953/DC1/.

Acknowledgments

The authors gratefully acknowledge financial support from the Research Council for the Chemical Sciences of the Netherlands Organization for Scientific Research (NWO-CW).

Received: December 24, 2004
Revised: April 23, 2005
Accepted: April 23, 2005
Published: July 12, 2005

References

Baca, M., Borgstahl, G.E.O., Boissinot, M., Burke, P.M., Williams, D.R., Slater, K.A., and Getzoff, E.D. (1994). Complete chemical structure of photoactive yellow protein: novel thioester-linked 4-hydroxycinnamyl chromophore and photocycle chemist. Biochemistry *33*, 14369–14377.

Bai, Y., Englander, J.J., Mayne, L., Milne, J.S., and Englander, S.W. (1995). Thermodynamic parameters from hydrogen exchange measurements. Methods Enzymol. *259*, 344–356.

Bai, Y., Milne, J.S., Mayne, L., and Englander, S.W. (1993). Primary structure effects on peptide group hydrogen exchange. Proteins *17*, 75–86.

Bonvin, A.M.J.J., and Brunger, A.T. (1996). Do NOE distances contain enough information to assess the relative populations of multi-conformer structures? J. Biomol. NMR *7*, 72–76.

Borgstahl, G.E.O., Williams, D.R., and Getzoff, E.D. (1995). 1.4 angstrom structure of photoactive yellow protein, a cytosolic photoreceptor: unusual fold, active-site, and chromophore. Biochemistry *34*, 6278–6287.

Brunger, A.T., Adams, P.D., Clore, G.M., DeLano, W.L., Gros, P., Grosse-Kunstleve, R.W., Jiang, J.S., Kuszewski, J., Nilges, M., Pannu, N.S., et al. (1998). Crystallography & NMR system: A new software suite for macromolecular structure determination. Acta Crystallogr. D Biol. Crystallogr. *54*, 905–921.

Corchnoy, S.B., Swartz, T.E., Lewis, J.W., Szundi, I., Briggs, W.R., and Bogomolni, R.A. (2003). Intramolecular proton transfers and structural changes during the photocycle of the LOV2 domain of phototropin 1. J. Biol. Chem. *278*, 724–731.

Cornilescu, G., Delaglio, F., and Bax, A. (1999). Protein backbone angle restraints from searching a database for chemical shift and sequence homology. J. Biomol. NMR *13*, 289–302.

Craven, C.J., Derix, N.M., Hendriks, J., Boelens, R., Hellingwerf, K.J., and Kaptein, R. (2000). Probing the nature of the blue-shifted intermediate of photoactive yellow protein in solation by NMR: hydrogen-deuterium exchange data and pH studies. Biochemistry *39*, 14392–14399.

Crews, S.T., Thomas, J.B., and Goodman, C.S. (1988). The *Drosophila* single-minded gene encodes a nuclear protein with sequence similarity to the per gene product. Cell *52*, 143–151.

Crosson, S., Rajagopal, S., and Moffat, K. (2003). The LOV domain family: photoresponsive signaling modules coupled to diverse output domains. Biochemistry *42*, 2–10.

Delaglio, F., Grzesiek, S., Vuister, G.W., Zhu, G., Pfeifer, J., and Bax, A. (1995). Nmrpipe: a multidimensional spectral processing system based on Unix pipes. J. Biomol. NMR *6*, 277–293.

Devanathan, S., Genick, U.K., Canestrelli, I.L., Meyer, T.E., Cusanovich, M.A., Getzoff, E.D., and Tollin, G. (1998). New insights into the photocycle of *Ectothiorhodospira halophila* photoactive yellow protein: photorecovery of the long-lived photobleached intermediate in the Met100Ala mutant. Biochemistry *37*, 11563–11568.

Düx, P., Rubinstenn, G., Vuister, G.W., Boelens, R., Mulder, F.A.A., Hard, K., Hoff, W.D., Kroon, A.R., Crielaard, W., Hellingwerf, K.J., and Kaptein, R. (1998). Solution structure and backbone dynamics of the photoactive yellow protein. Biochemistry *37*, 12689–12699.

Farrow, N.A., Muhandiram, D.R., Singer, A.U., Pascal, S.M., Kay, C.M., Gish, G., Shoelson, S.E., Pawson, T., Forman-Kay, J.D., and Kay, L.E. (1994). Backbone Dynamics of a free and a phosphopeptide-complexed Src homology 2 domain studied by ^{15}N NMR relaxation. Biochemistry *33*, 5984–6003.

Fedorov, R., Schlichting, I., Hartmann, E., Domratcheva, T., Fuhrmann, M., and Hegemann, P. (2003). Crystal structures and molecular mechanism of a light-induced signaling switch: the Phot-LOV1 domain from *Chlamydomonas reinhardtii*. Biophys. J. *84*, 2474–2482.

Garcia de la Torre, J., Huertas, M.L., and Carrasco, B. (2000). HYDRONMR: prediction of NMR relaxation of globular proteins from atomic-level structures and hydrodynamic calculations. J. Magn. Reson. *147*, 138–146.

Genick, U.K., Borgstahl, G.E.O., Ng, K., Ren, Z., Pradervand, C., Burke, P.M., Srajer, V., Teng, T.Y., Schildkamp, W., McRee, D.E., et al. (1997). Structure of a protein photocycle intermediate by millisecond time-resolved crystallography. Science *275*, 1471–1475.

Harper, S.M., Neil, L.C., and Gardner, K.H. (2003). Structural basis of a phototropin light switch. Science *301*, 1541–1544.

Hendriks, J., Gensch, T., Hviid, L., van der Horst, M.A., Hellingwerf, K.J., and van Thor, J.J. (2002). Transient exposure of hydrophobic surface in the photoactive yellow protein monitored with Nile red. Biophys. J. *82*, 1632–1643.

Hoff, W.D., Düx, P., Hard, K., Devreese, B., Nugterenroodzant, I.M., Crielaard, W., Boelens, R., Kaptein, R., Vanbeeumen, J., and Hellingwerf, K.J. (1994a). Thiol ester-linked P-Coumaric acid as a new photoactive prosthetic group in a protein with rhodopsin-like photochemistry. Biochemistry *33*, 13959–13962.

Hoff, W.D., Vanstokkum, I.H.M., Vanramesdonk, H.J., Vanbrederode, M.E., Brouwer, A.M., Fitch, J.C., Meyer, T.E., Vangrondelle, R., and Hellingwerf, K.J. (1994b). Measurement and global analysis of the absorbency changes in the photocycle of the photoactive yellow protein from *Ectothiorhodospira halophila*. Biophys. J. *67*, 1691–1705.

Hoffman, E.C., Reyes, H., Chu, F.F., Sander, F., Conley, L.H., Brooks, B.A., and Hankinson, O. (1991). Cloning of a factor required for activity of the Ah (dioxin) receptor. Science *252*, 954–958.

Imamoto, Y., Kamikubo, H., Harigai, M., Shimizu, N., and Kataoka, M. (2002). Light-induced global conformational change of photoactive yellow protein in solution. Biochemistry *41*, 13595–13601.

Johnson, B.A., and Blevins, R.A. (1994). NMRView: a computer program for the visualization and analysis of NMR data. J. Biomol. NMR *4*, 603–614.

Jorgensen, W.L., and Tiradorives, J. (1988). The OPLS potential functions for proteins: energy minimizations for crystals of cyclicpeptides and crambin. J. Am. Chem. Soc. *110*, 1666–1671.

Korzhnev, D.M., Skrynnikov, N.R., Millet, O., Torchia, D.A., and Kay, L.E. (2002). An NMR experiment for the accurate measurement of heteronuclear spin-lock relaxation rates. J. Am. Chem. Soc. *124*, 10743–10753.

Laskowski, R.A., Rullmann, J.A.C., MacArthur, M.W., Kaptein, R., and Thornton, J.M. (1996). AQUA and PROCHECK-NMR: programs for checking the quality of protein structures solved by NMR. J. Biomol. NMR *8*, 477–486.

Linge, J.P., O'Donoghue, S.I., and Nilges, M. (2001). Automated assignment of ambiguous nuclear Overhauser effects with ARIA. Methods Enzymol. *339*, 71–90.

Linge, J.P., Williams, M.A., Spronk, C.A.E.M., Bonvin, A.M.J.J., and Nilges, M. (2003). Refinement of protein structures in explicit solvent. Proteins *50*, 496–506.

Meiboom, S., and Gill, D. (1958). Modified spin-echo method for measuring nuclear relaxation times. Rev. Sci. Instrum. *29*, 688–691.

Meyer, T.E. (1985). Isolation and characterization of soluble cytochromes, ferredoxins and other chromophoric proteins from the halophilic phototrophic bacterium *Ectothiorhodospira halophila*. Biochim. Biophys. Acta *806*, 175–183.

Meyer, T.E., Yakali, E., Cusanovich, M.A., and Tollin, G. (1987). Properties of a water-soluble, yellow protein isolated from a halophilic phototrophic bacterium that has photochemical activity analogous to sensory rhodopsin. Biochemistry *26*, 418–423.

Pellequer, J.L., Wager-Smith, K.A., Kay, S.A., and Getzoff, E.D. (1998). Photoactive yellow protein: a structural prototype for the three-dimensional fold of the PAS domain superfamily. Proc. Natl. Acad. Sci. USA *95*, 5884–5890.

Peng, J.W., Thanabal, V., and Wagner, G. (1991). 2D Heteronuclear NMR measurements of spin-lattice relaxation-times in the rotating frame of X nuclei in heteronuclear HX spin systems. J. Magn. Reson. *94*, 82–100.

Rubinstenn, G., Vuister, G.W., Mulder, F.A.A., Düx, P.E., Boelens, R., Hellingwerf, K.J., and Kaptein, R. (1998). Structural and dynamic changes of photoactive yellow protein during its photocycle in solution. Nat. Struct. Biol. *5*, 568–570.

Rubinstenn, G., Vuister, G.W., Zwanenburg, N., Hellingwerf, K.J., Boelens, R., and Kaptein, R. (1999). NMR experiments for the study of photointermediates: application to the photoactive yellow protein. J. Magn. Reson. *137*, 443–447.

Salomon, M., Eisenreich, W., Durr, H., Schleicher, E., Knieb, E., Massey, V., Rudiger, W., Muller, F., Bacher, A., and Richter, G. (2001). An optomechanical transducer in the blue light receptor phototropin from *Avena sativa*. Proc. Natl. Acad. Sci. USA *98*, 12357–12361.

Sattler, M., Schleucher, J., and Griesinger, C. (1999). Heteronuclear multidimensional NMR experiments for the structure determination of proteins in solution employing pulsed field gradients. Progress in Nuclear Magnetic Resonance Spectroscopy *34*, 93–158.

Sprenger, W.W., Hoff, W.D., Armitage, J.P., and Hellingwerf, K.J. (1993). The eubacterium *Ectothiorhodospira halophila* is negatively phototactic, with a wavelength dependence that fits the absorption-spectrum of the photoactive yellow protein. J. Bacteriol. *175*, 3096–3104.

Swartz, T.E., Wenzel, P.J., Corchnoy, S.B., Briggs, W.R., and Bogomolni, R.A. (2002). Vibration spectroscopy reveals light-induced chromophore and protein structural changes in the LOV2 domain of the plant blue-light receptor phototropin 1. Biochemistry *41*, 7183–7189.

Takeshita, K., Imamoto, Y., Kataoka, M., Tokunaga, F., and Terazima, M. (2002). Themodynamic and transport properties of intermediate states of the photocyclic reaction of photoactive yellow protein. Biochemistry *41*, 3037–3048.

Taylor, B.L., and Zhulin, I.B. (1999). PAS domains: internal sensors of oxygen, redox potential, and light. Microbiol. Mol. Biol. Rev. *63*, 479–506.

van der Horst, M.A., van Stokkum, I.H., Crielaard, W., and Hellingwerf, K.J. (2001). The role of the N-terminal domain of photoactive yellow protein in the transient partial unfolding during signalling state formation. FEBS Lett. *497*, 26–30.

Vreede, J., van der Horst, M.A., Hellingwerf, K.J., Crielaard, W., and van Aalten, D.M.F. (2003). PAS domains: common structure and common flexibility. J. Biol. Chem. *278*, 18434–18439.

Vreede, J., Crielaard, W., Klaas, J., Hellingwerf, K.J., and Bolhuis, P.G. (2005). Predicting the signaling state of photoactive yellow protein. Biophysi. J. *88*, 3525–3535.

Zwahlen, C., Legault, P., Vincent, S.J.F., Greenblatt, J., Konrat, R., and Kay, L.E. (1997). Methods for measurement of intermolecular NOEs by multinuclear NMR spectroscopy: application to a bacteriophage lambda N-peptide/boxB RNA complex. J. Am. Chem. Soc. *119*, 6711–6721.

Accession Numbers

The structural coordinates have been deposited in the Protein Data Bank with the following accession codes: 1XFN for pG and 1XFQ for pB.